Supporting information

Hierarchical Polyaromatic Hydrocarbons (PAH) with Superior Sodium Storage Properties

Jie Qu[a,b,c], Xin-Xin Dai[b], Jie-Shun Cui[b], Rou-Xi Chen[b], Xin Wang[d], Yen-Hao Lin[e],

Rafael Verduzco[e], Hsing-Lin Wang[a,b,c,*]

a. *Shenzhen Key Laboratory of Solid State Batteries, Southern University of Science and Technology, Shenzhen 518055, China*
b. *Department of Materials Science and Engineering, Southern University of Science and Technology, Shenzhen, 518055, China.*
c. *Guangdong Provincial Key Laboratory of Energy Materials for Electric Power, Southern University of Science and Technology, Shenzhen 518055, China*
d. *Academy for Advanced Interdisciplinary Studies & Department of Physics, Southern University of Science and Technology, Shenzhen, Guangdong, 518055, China*
e. *Department of Chemical and Biomolecular Engineering, Rice University, Houston TX, 77005, United States.*

Materials Preparation:

The HBC and HBC-OMe samples were synthesized with a multistep solution-chemistry route.[1]

1. The synthesis of HPB-H

Compounds tris[4-(2-phenylethynyl)phenyl)]amine (Ph$_3$TPA) and tris(4-((4-tert-butylphenyl)ethynyl)phenyl)amine (tBu$_3$TPA) were synthesized by threefold Sonogashira coupling of the triiodo compound tris(4-iodophenyl)amine (I3TPA) with phenylacetylene and 4-tert-butylphenylacetylene, respectively.

2. The synthesis of HPB-OMe

A mixture of tris[4-(2-phenylethynyl)phenyl)] amine (Ph$_3$TPA)and 3,4-bis-(4-methoxyphenyl)-2,5-diphenyl-cyclopenta-2,4-dienone (TPCP-OMe) in Ph$_2$O (35 mL) was purged with N$_2$ and heated at reflux for 24 h. The mixture was cooled, MeOH (200 mL) was added, and the resulting solid was separated by filtration. The product was re-precipitated by dicholomethane/MeOH to afford purified **HPB-OMe** as a beige powder (6.70 g, 94%).

3. The synthesis of HBCs

The as-synthesized HPBs were then planarized (fusion of benzene rings) by treating with FeCl$_3$ in a dichloromethane/nitromethane mixture for 2–3 h to form the corresponding HBCs. After quenched the reaction with methanol, repetitive dissolution and precipitation with dichloromethane/methanol yielded aimed products.
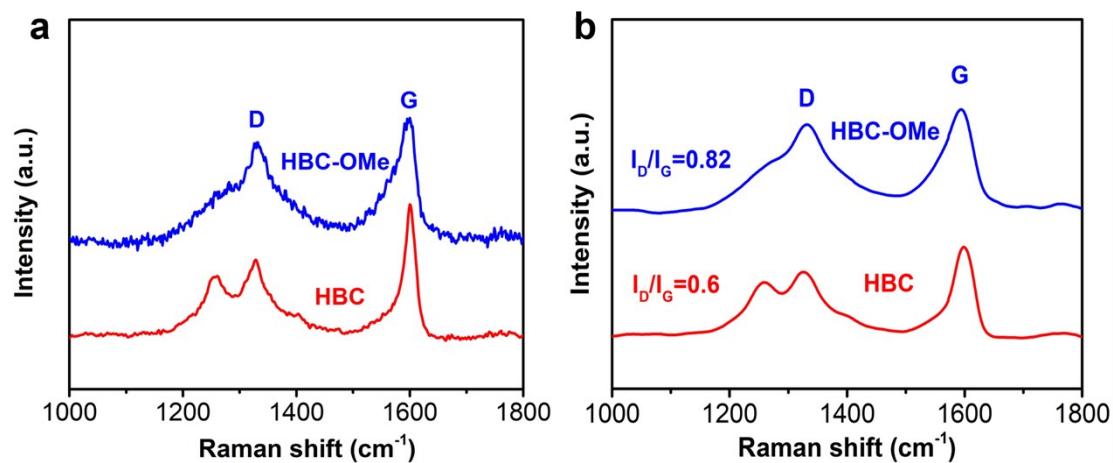
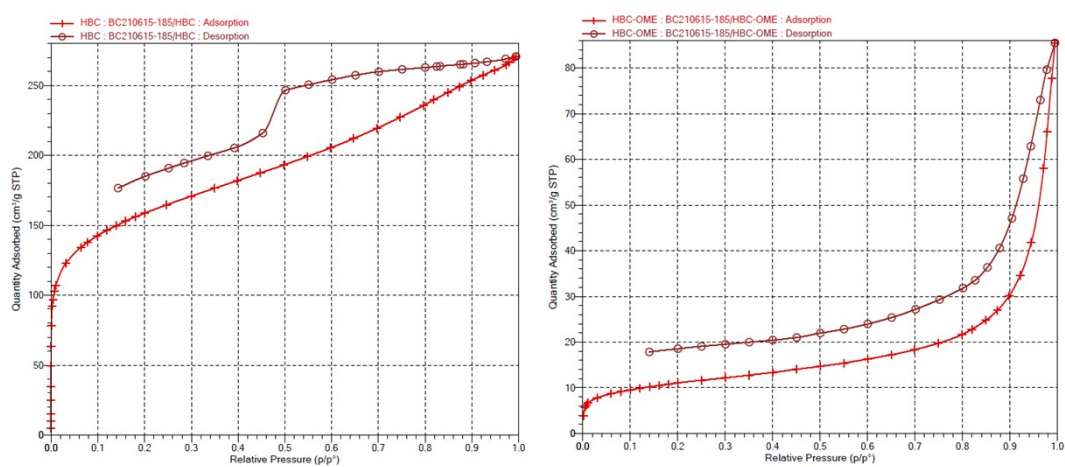**Figure S1**. Pristine (a) and fitted (b) Raman spectra of HBC and HBC-OMe sample.

Figure S2. N_2 sorption isotherms (at 77 K) for the activated samples of HBC (left) and HBC-OMe (right).
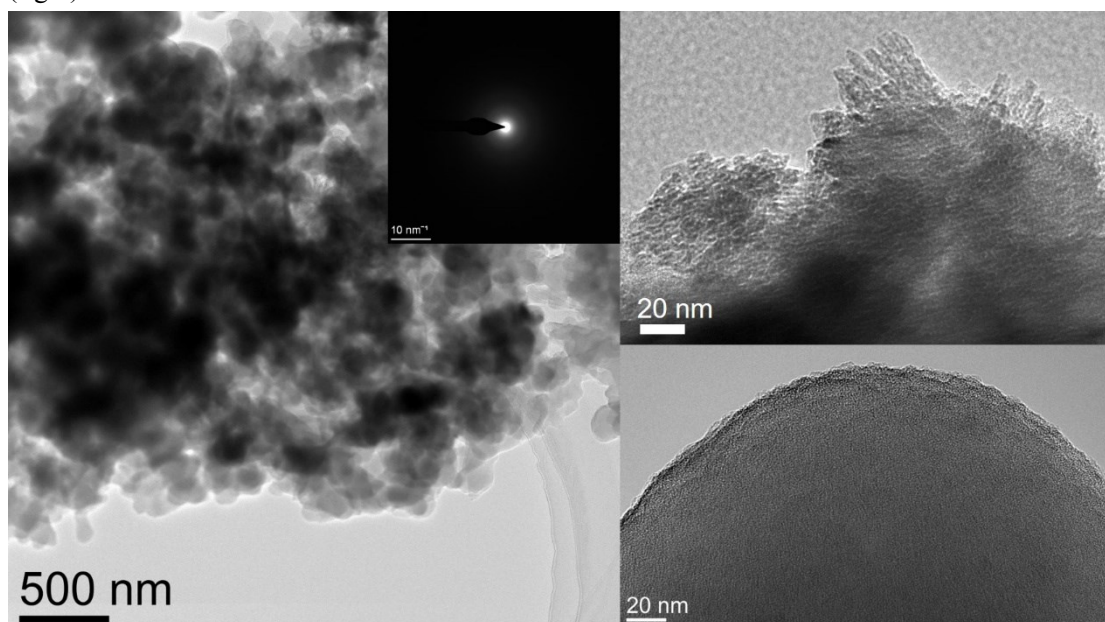

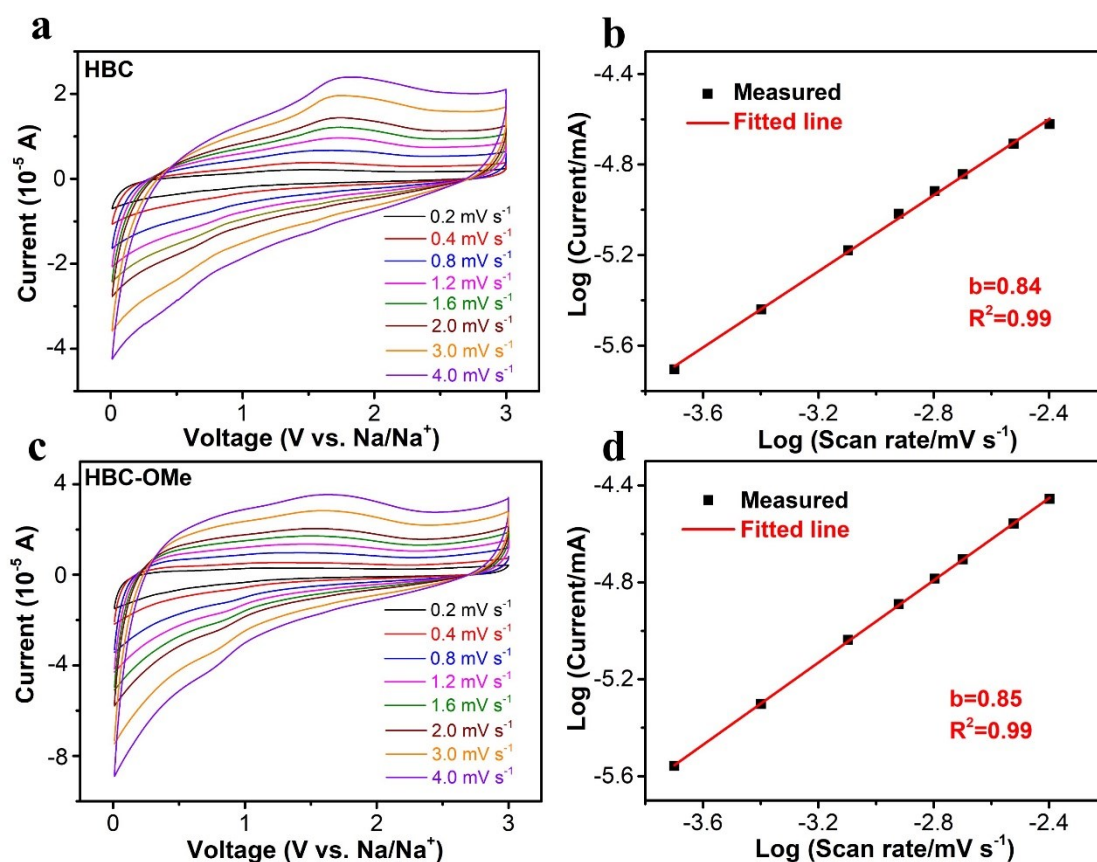**Figure S3**. HRTEM images of HBC-OMe sample

Figure S4. CV plots at the scan rate from 0.2 mV s-1 to 4.0 mV s-1 (a, c); Linear relationship between the Log (Current) and the Log (Scan rate) for HBC (c) and HB-OMe (d).

The CV curves at different scan rates are exhibited in Figure S3a and c, which show similar rectangle-shape plots, suggesting analogous electrochemical behavior. According to the power law relationship between scan rate v and current i, the degree of capacitive effect can be qualitatively analyzed ($i = a^v b$, where a and b are constants, $b = 0.5$ and 1.0 stands for the diffusion-controlled process and capacitive-induced process, respectively). As shown in Figure S3b and d, the b values for HBC and HBC-OMe electrode are 0.84 and 0.85, respectively, suggesting the capacity contribution is largely originated from the capacitive-dominated process.
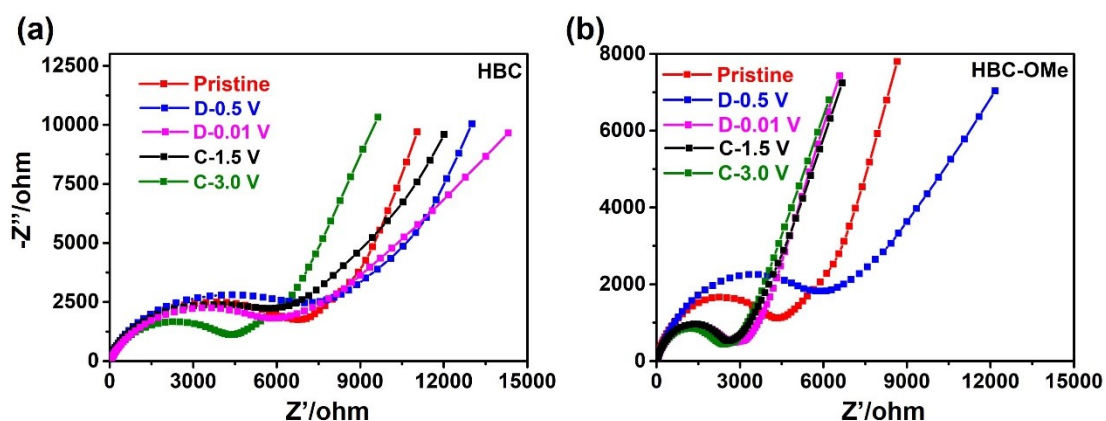
Figure S5. EIS analysis of HBC (a) and HBC-OMe (b) for various charging and discharging states.

Electrochemical impedance spectroscopy (EIS) technique was used to investigate the kinetic performances during electrochemical desodiation process. As shown in **Figure S3**, the Nyquist profiles are comprised of two different regions, one is semicircle located in the high-medium frequency range, which is associated to the charge-transfer resistance (Rct), and the other straight line in the low frequency region is ascribed to the Na$^+$ diffusion in the electrode. As shown in Figure Sa, for HBC electrodes, obviously, compared with the pristine electrode, the diameter of the semicircle increased rapidly when discharged to 0.5 V and slowly decreased when discharged to 0.01 V, indicating the speedy increasing Rct during discharging process, which could be originated from the SEI film formation and the electrolyte activation, in great accordance with the CV and GDC test results discussed above. The Rct apparently declined during charging process, which demonstrates that the SEI layer has been gradually stable until the end the first discharging process. The Rct of HBC-OMe electrodes display similar change trend during different charging and discharging states. Interestingly, when charged to 3.0 V, the Rct of HBC-OMe electrode is much smaller than that of HBC electrode, implying the faster electrical conductivity, which is closely consistent with rate capability.

Table S1. Elemental compositions of the as-prepared sample from the XPS data

Sample	C (at.%)	N (at.%)	O (at.%)
HBC	97.92	2.08	0
HBC-OMe	82.21	1.56	16.23

Table S2. The electrochemical performances comparisons of carbon electrodes in SIBs.

Materials	Capacity (mAh g^{-1})/current density (A g^{-1})	Rate performance (mAh g^{-1})/current density (A g^{-1})	Cycling stability (cycles, current density)	Ref.
HBC-OMe	**506 / 0.1**	**217 / 5** **161 / 10**	**290 mAh g^{-1}** **(1000, 2A g^{-1})**	**This work**
N-rich graphene	264.3 / 0.1	148 / 5 114 / 10	210 mAh g^{-1} (2000, 0.5 A g^{-1})	[2]
N-doped graphene	494 / 0.1	262 / 2	189 mAh g^{-1} (500, 0.5 A g^{-1})	[3]
Graphite microcrystal/ graphene composites	279 / 0.05	131 / 2	101 mAh g^{-1} (2000, 2 A g^{-1})	[4]
Reduced holy graphene oxide	365 / 0.1	131 / 10	163 mAh g^{-1} (3000, 2 A g^{-1})	[5]
Holey graphene nanosheets	220 / 0.03	85 / 10	186 mAh g^{-1} (500, 0.1 A g^{-1})	[6]
S-Doped graphene	436 / 0.05	217 / 3.2	250 mAh g^{-1} (1000, 2 A g^{-1})	[7]
Flexible hard carbon	372 / 0.03	256 / 0.1	180 mAh g^{-1} (500, 0.2 A g^{-1})	[8]
Carbon quantum dots	290 / 0.2	130 / 5 104 / 10	188 mAh g^{-1} (500, 2.5 A g^{-1})	[9]
Hard carbon	186 / 0.25	86 / 2.5	\	[10]
P-doped hard carbon	346 / 0.02	67 / 1	290 mAh g^{-1} (150, 0.04 A g^{-1})	[11]
P-doped hard carbon nanofibers	287 / 0.05	103 / 2	253 mAh g^{-1} (200, 0.05 A g^{-1})	[12]
Expanded graphite	284 / 0.02	91 / 0.2	150 mAh g^{-1} (2000, 0.1 A g^{-1})	[13]
Edge-nitrogen-rich carbon dots pillared graphene	348 / 0.1	118 / 10	253 mAh g^{-1} (3000, 0.3 A g^{-1})	[14]

Reference

[1] M. G. Schwab, A. Narita, Y. Hernandez, T. Balandina, K. S. Mali, S. De Feyter, X. Feng, K. Müllen, *J. Am. Chem. Soc*. **2012**, *134*, 18169.

[2] J. L. Liu, Y. Q. Zhang, L. Zhang, F. X. Xie, A. Vasileff, S. Z. Qiao, *Adv. Mater.* **2019**, *31*, 1901261.

[3] Y. Yang, Z. Z. Pan, Y. Y. Wang, Y. C. Ma, C. L, Y. J. Lu, X. L. Wu, *Nanoscale*. **2019**, *11*, 14616.

[4] M. M. Kang, H. Q. Zhao, J. Q. Ye, W. Song, H. T. Shen, J. Mi, Z. Li, *J. Mater. Chem. A*. **2019**, *7*, 7565.

[5] J. Zhao, Y. Z. Zhang, F. Zhang, H. F. Liang, F. W. Ming, H. N. Alshareef, Z. Q. Ga, *Adv. Energy Mater.* **2019**, *9*, 1803215.

[6] X. F. Luo, C. H. Yang, J. K. Chang, *J. Mater. Chem. A*, **2015, 3**, 17282.

[7] B. Quan, A. Jin, S. H. Yu, S. K. Kang, J. Jeong, H. D. Abruna, L. Y. Jin, Y. Z. Piao, Y. E. Sung, *Adv. Sci.* **2018**, *5*, 1700880.

[8] N. Sun, Y. B. Guan, Y. T. Liu, Q. Z. Zhu, J. R. Shen, H. Liu, S. Q. Zhou, B. Xu, *Carbon*. **2018**, *137*, 475.

[9] H. S. Hou, C. E. Banks, M. J. Jing, Y. Zhang, X. B. Ji, *Adv. Mater.* **2015**, *27*, 7861.

[10] Z. F. Li, Z. L. Jian, X. F. Wang, I. A. Rodri´guez-Pe´rez, *Chem. Commun.* 2017, *53*, 2610.

[11] Z. Li, L. Ma, T. W. Surta, C. Bommier, Z. Jian, Z. Xing, W. F. Stickle, M. Dolgos, K. Amine, J. Lu, T. Wu, X. Ji, *ACS Energy Lett.* **2016**, *1*, 395.

[12] F. Wu, R. Dong, Y. Bai, Y. Li, G. Chen, Z. Wang, C. Wu, *ACS Appl. Mater. Interfaces.* **2018**, *10*, 21335.

[13] Y. Wen, K. He, Y. Zhu, F. Han, Y. Xu, I. Matsuda, Y. Ishii, J. Cumings, C. Wang, *Nat. Commun.* **2014**, *5*, 4033.

[14] Z. Liu, L. Zhang, L. Sheng, Q. Zhou, T. Wei, J. Feng, Z. Fan, *Adv. Energy Mater.* **2018**, *8*, 1802042.